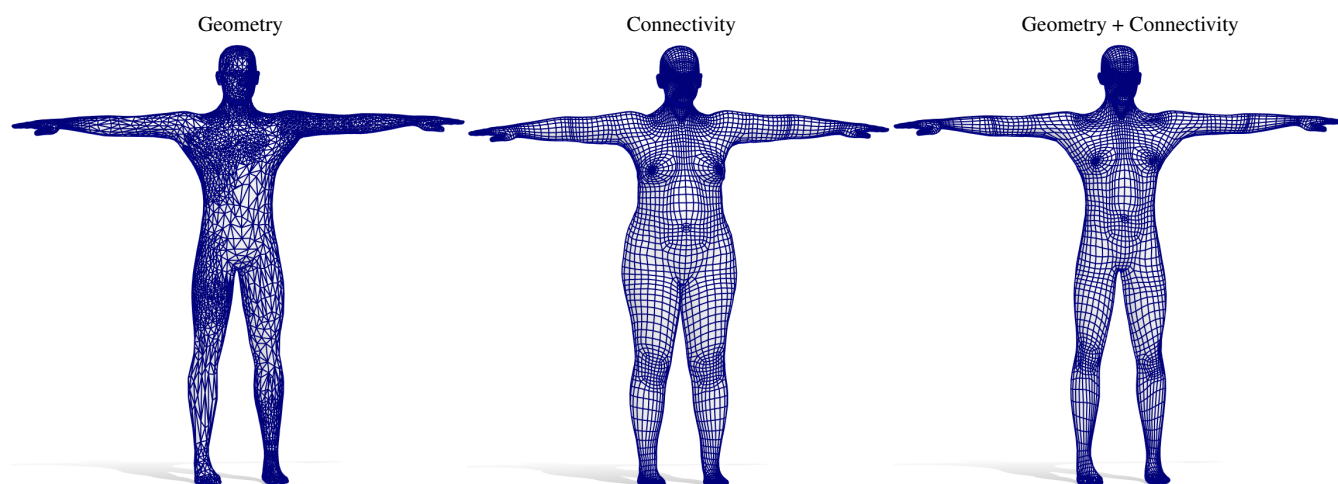# CMH: Coordinates Manifold Harmonics for Functional Remeshing

R. Marin[1][†], S. Melzi[1] [†] , P. Musoni[2], F. Bardon[1], M. Tarini[2], U. Castellani[1]

[1]University of Verona, Italy   [2]University of Milano, Italy

Figure 1: *An example of the mesh transfer provided by the CMH pipeline. From left to right: the shape with the desired geometry, the desired mesh connectivity, the mesh transferred through the proposed method providing the desired connectivity on the desired geometry.*

Abstract
In digital world reconstruction, 2-dimensional surface of real objects are often obtained as polygonal meshes after an acquisition procedure using 3D sensors. However, such representation requires several manual efforts from highly experts to correct the irregularity of tessellation and make it suitable for professional applications, such as those in the gaming or movie industry. Moreover, for modelling and animation purposes it is often required that the same connectivity is shared among two or more different shapes. In this paper we propose a new method that exploits a remeshing-by-matching *approach where the observed noisy shape inherits a regular tessellation from a target shape which already satisfies the professional constraints. A fully automatic pipeline is introduced based on a variation of the functional mapping framework. In particular, a new set of basis functions, namely the* Coordinates Manifold Harmonics *(CMH), is properly designed for this tessellation transfer task. In our experiments an exhaustive quantitative and quality evaluation is reported for human body shapes in T-pose where the effectiveness of the proposed functional remeshing is clearly shown in comparison with other methods.*

CCS Concepts
*• **Mathematics of computing** → **Functional analysis**; • **Computing methodologies** → Shape analysis; • **Theory of computation** → Computational geometry;*

1. Introduction

The research on effective virtual representation of real objects and scenes is one of the main topic in modern computer graphics. The attention on this task has greatly grown in the last decades due to the rapid improvement and versatility of the available devices for the acquisition of geometric information from the real world. In this context, the most preferred data representation consists of polygonal meshes where the quality of mesh tessellation is very important for modelling and animation purposes. For instance the density of polygons must be higher in the surface areas with more geometric details such as around the mouth of the eyes of a human face. Fur-

[†] Equal Contribution

thermore, the orientation of the polygon edges must be properly defined to improve the animation of articulated objects. Unfortunately, the meshes obtained from 3D scans are highly irregular and require a lot of manual efforts to be used by professional artists. Automatic remeshing methods alleviate this issue but the performance of these approaches are still not sufficient. Moreover, it is often required that a tessellation is coherent among a set of different shapes. Some works for co-tessellation between pairs of objects have been recently proposed but their performance is limited and no one has become a consolidated standard.

In this paper we propose a new fully automatic method for object tessellation using a *remeshing-by-matching* approach where a regular mesh of a target shape is transferred to the surface of the observed shape. The overall idea is depicted in Figure 1. The observed object (left) is represented with a highly irregular triangular mesh (e.g., the density of triangles are not coherent between the left and right side of the human body and the areas with more triangles are randomly distributed). The target object (center) is encoded by a regular mesh that satisfies the request of a technical artist (e.g., the tessellation is fully symmetric and the density of triangles is more concentrated around the surface details). Finally, the output of our remeshing (right) is the source shape with the target tessellation. In this fashion we keep the underlying geometry from the observed (i.e., irregular) object and inherit the surface sampling and vertex connectivity from the target (i.e., regular) shape. To this aim, we need an accurate and procedure for point-to-surface matching. Our approach focuses on the functional shape matching framework that is independent from rigid transformations of the 3D space and robust to the surface discretization. In particular, we propose a new set of orthonormal functions that we call *Coordinates Manifold Harmonics* (CMH) properly designed to make the functional map estimation more efficient and reliable for mesh transfer. We emphasize here that we are not looking for an optimal set of basis function with respect to some energy, instead we are proposing an intuitive method that is able to inject the extrinsic information in an intrinsic pipeline. Moreover, we exploit the *as rigid as possible* (ARAP) constraint to further refine the regular properties of the output.

2. Related works

In this Section we briefly introduce the existing methods that are more closely related with our work: i) shape matching by functional map, and ii) surface remeshing.

The functional maps framework was firstly proposed by Ovsjanikov et al. in [OBCS*12] and represents the state of the art for shape matching. The peculiarity of this method is to revise the estimation of correspondences in the functional space exploiting the effectiveness of spectral shape analysis. The main positive properties of functional maps are the compactness, the computation efficiency and their ability to transfer information among shapes. More recently, several advances have been introduce to improve the functional maps computation [NMR*18, EBC17] and functional spaces representation [MRCB18, NO17]. [NMR*18] presents an extension of functional maps framework, considering the problem of pointwise product preservation. [EBC17] includes methods for functional maps denoising and deblurring. Some alternatives to the Laplace-Beltrami basis was proposed in [MRCB18] to provide

a theoretical foundation of the Hamiltonian Operator [CSBK16] for different shape analysis tasks, in [NO17] to improve the map quality by function products preservation, and in [AK17] to define geometry regularization for the PCA basis. Interestingly, functional maps have been exploited for tangent vector fields mapping [ABCCO13] to generate a consistent quadrangulation among pair of shapes [ACBCO17]. Our work is strongly related to this cotesellation method. We differ from [ACBCO17] since we propose a different functional map strategy and we have a full control of the output mesh.

The literature on surface re-meshing spans decades, and is extremely vast and a categorization is beyond scope of this work. A mesh is often required to be highly regular, featuring only few irregular vertices (**"semi-regular"** remeshing), or, more rarely, none at all: **"fully regular"** remeshing. The final resolution is preferred to be **adaptive**, devoting more vertices in more geometrically complex or more semantically important areas. **Edge orientation** and position is also important. Reproducing creases of surface as edges in the mesh is crucial for geometrical fidelity, in CAD models. More in general, edge must be oriented according to curvature directions or to arbitrary prescribed directions (also interactively so, e.g. [JTPSH15]). For **animated meshes** (e.g. skinned meshes, or blend shapes), edge orientation must adhere the intended deformations [MPP*13]. The re-meshing problem can be approached from drastically different angles, such as: interactively connecting an existing vertices of a point cloud with new triangles [BMR*99], by parametrizing the surface and then defining a regular tri or quad grid in the parametric space [BZK09], or by coarsening the orignial mesh and then regularly subdividing the resulting low-poly mesh [PTC10], just to mention a few. Another class of solutions, *example based re-meshing*, learns remeshing configuration from existing manually designed examples. This is reminiscent to our own approach in that good examples, e.g. meshes edited by artists, are leveraged to help the construction of new meshes [MTP*15]. In summary, in spite of a long history of advancement and breakthrough, surface remeshing is still an unsolved problem: manually designed meshes, constructed by trained digital artists, are still unmatched in terms of quality. For this reason, in the industry, the task of remeshing a given surface (e.g. a range scanned one), which is often termed "re-topology" in this context, is typically performed manually or semi-manually by trained digital artists.

3. Background

Main objects of this paper are the 2-dimensional surfaces embedded in $\mathbb{R}^3$. We represent this surface as a compact and connected smooth 2-dimensional Riemannian manifold $\mathcal{M} \subset \mathbb{R}^3$, eventually with a boundary $\partial\mathcal{M}$. A real-valued function f on $\mathcal{M}$ is a mapping from every point $x \in \mathcal{M}$ to $\mathbb{R}$ that associates at every point a real value. For brevity we avoid defining all the differential geometry theory that is needed to fully understand how to equip these surfaces of a "Fourier-like" basis for the representation of the functions defined on $\mathcal{M}$.

From differential geometry we obtain the definition of the *Laplace Beltrami Operator* (LBO) on $\mathcal{M}$. The LBO corresponds to the natural extension of the Laplacian Operator to non-Euclidean domains (the Laplacian is defined as the sum of second partial

derivatives of the function in each variable in Euclidean domains.) Since the LBO is a positive semidefinite operator $\boldsymbol{\Delta}_{\mathcal{M}} : L^2(\mathcal{M}) \to L^2(\mathcal{M})$, it has eigendecomposition $\boldsymbol{\Delta}_{\mathcal{M}} \boldsymbol{\phi}_l = \lambda_l \boldsymbol{\phi}_l$, where $\boldsymbol{\Phi} = \boldsymbol{\phi}_1, \boldsymbol{\phi}_2, \ldots$ are its eigenfunctions, $\boldsymbol{\Lambda} = \lambda_1 \leq \lambda_2 \leq \ldots$ are the corresponding eigenvalues and all these eigenvalues are real. The set of LBO eigenfunctions $\boldsymbol{\Phi}$ forms an orthonormal basis for $L^2(\mathcal{M})$, the space of square-integrable functions defined on $\mathcal{M}$. Functions in $\boldsymbol{\Phi}$ are usually referred to as *Manifold Harmonics* (MH) and can be seen as the Fourier basis on $\mathcal{M}$. The standard choice for a basis of $L^2(\mathcal{M})$ corresponds to the set of eigenfunctions corresponding to the smallest eigenvalues of the LBO. In the discrete setting we represent $\mathcal{M}$ as a triangular mesh $(\mathcal{V}, \mathcal{E})$, where $\mathcal{V}$ is the set of its $n_{\mathcal{M}}$ vertices and $\mathcal{E}$ is the list of its edges. The LBO is this setting is represented by a matrix of dimension $n_{\mathcal{M}} \times n_{\mathcal{M}}$. This matrix is defined as $\boldsymbol{\Delta}_{\mathcal{M}} = (\boldsymbol{A}^{\mathcal{M}})^{-1} \boldsymbol{W}^{\mathcal{M}}$, where $\boldsymbol{A}^{\mathcal{M}}$ is the *mass matrix* and $\boldsymbol{W}^{\mathcal{M}}$ is the *stiffness matrix*. The mass matrix is a diagonal matrix whose entries are equal to the area element associated to each vertex. The stiffness matrix represents the local geometry. We define the stiffness matrix through the cotangent scheme, we refer to [PP93] for further details.

Functional Maps. Consider two shapes $\mathcal{N}$ and $\mathcal{M}$, and let $\boldsymbol{\Pi} : \mathcal{N} \to \mathcal{M}$ be a pointwise map between them. Classical shape matching approaches try to identify directly the point-to-point correspondences (i.e., solve for the map $\boldsymbol{\Pi}$). The functional maps approach [OBCS*12] solve first for a functional correspondence and then extract a point-to-point correspondence from the functional one. First of all functional maps considers a linear operator $T : L^2(\mathcal{M}) \to L^2(\mathcal{N})$ mapping *functions* defined on $\mathcal{M}$ to *functions* on $\mathcal{N}$, defined as the composition $T(\boldsymbol{f}) = \boldsymbol{f} \circ \boldsymbol{\Pi}, \forall \boldsymbol{f} \in L^2(\mathcal{M})$. Given a pair of basis $\boldsymbol{\Phi} = \{\boldsymbol{\phi}_i\}$ and $\boldsymbol{\Psi} = \{\boldsymbol{\psi}_j\}$ respectively for $L^2(\mathcal{M})$ and $L^2(\mathcal{N})$ The operator T can be compactly represented as matrix $\boldsymbol{C} = (c_{hl})$, where the coefficients c_{hl} are defined according to:

$$T(\boldsymbol{f}) = T \sum_i \langle \boldsymbol{f}, \boldsymbol{\phi}_l \rangle_{\mathcal{M}} \boldsymbol{\phi}_l = \sum_{lh} \langle \boldsymbol{f}, \boldsymbol{\phi}_l \rangle_{\mathcal{M}} \underbrace{\langle T\boldsymbol{\phi}_l, \boldsymbol{\psi}_h \rangle_{\mathcal{N}}}_{c_{hl}} \boldsymbol{\psi}_h. \quad (1)$$

As said before usually the adopted basis are the eigenfunctions of the the LBO. As suggested in [OBCS*12], the series (1) can be truncated after the first $k_{\mathcal{M}}$ and $k_{\mathcal{N}}$ coefficients, yielding a low-pass approximation (in the Fourier sense) of the underlying map $\boldsymbol{\Pi}$. Estimating a low-rank functional map in the Fourier basis thus boils down to solving for a matrix $\boldsymbol{C} \in \mathbb{R}^{k_{\mathcal{N}} \times k_{\mathcal{M}}}$, as opposed to the classical full correspondence (and usually binary) matrix $\Pi \in \mathbb{R}^{n_{\mathcal{M}} \times n_{\mathcal{N}}}$ ($n_{\mathcal{M}}$ and $n_{\mathcal{N}}$ are the number of vertices in the discrete setting respectively of $\mathcal{M}$ and $\mathcal{N}$), where typically $k_{\mathcal{M}}$ and $k_{\mathcal{N}} \ll n$. More details about functional maps can be found in [OCB*16].

4. Method

In this Section we outline the proposed method. Given a triangular mesh $\mathcal{S} = (\mathcal{V}, \mathcal{E})$, our main goal is to automatically transfer the connectivity of $\mathcal{S}$ on the geometry represented by a new shape $\mathcal{M}$.

Motivations. The functional map framework introduced in 3 is a clever and efficient approach for solving the point-to-point matching. It is completely independent from the shapes representation and its performance are unrelated by the number of points that are
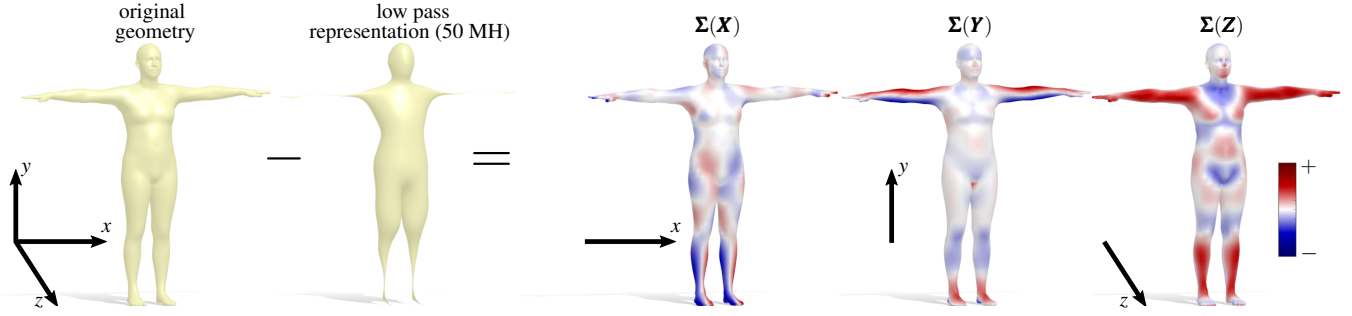
original geometry | representation with 106 MH | representation with 53 CMH
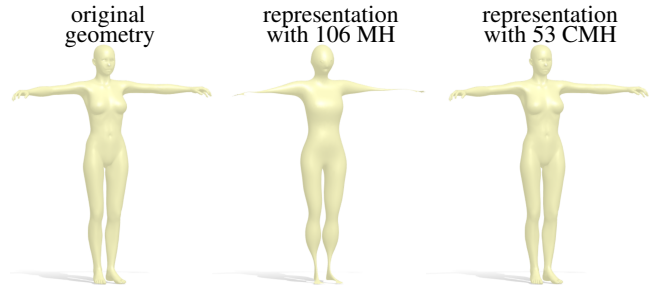
Figure 2: *Comparison between the geometry representation provided by* 106 *standard MH and the proposed* 53 *CMH. From left to right: the original shape, the low-pass representation provided by* 106 *MH and our geometry representation.*

sampled on the surface. However, it suffers from a strong limitation. The functional map $\boldsymbol{C}$ is estimated through the minimization problem in Equation 1, where the number of unknowns are exactly $k_{\mathcal{S}} k_{\mathcal{M}}$. These numbers also define the frequencies that are involved in the mapping, in other words the larger are $k_{\mathcal{S}}$ and $k_{\mathcal{M}}$ the wider is the low-band filter that is applied on the functions representation. This relation generates a trade-off for the functional maps frameworks: to allow the framework to represent the higher frequencies correctly a more complex optimization problem should be solved (and viceversa). In literature, the standard choices for $k_{\mathcal{S}}$ and $k_{\mathcal{M}}$ are $30, 60, 100$ while 200 or 300 are already considered too much large values. On the other hand, as can be seen in the center of Figure 2, with $k_{\mathcal{S}} = 106$ the representation of the geometry is very poor and many details are lost. This lack of quality motivates our definition of the *CMH basis*. Our models are able to represent the geometry of the given shapes just by adding three functions to a fixed set of standard manifold harmonics. An example of the representation provided by CMH is depicted on the right of Figure 2. As we will show in the Section 5 adopting the CMH instead of the standard MH we are able to improve the representation of high frequency details adding only few more variables in the optimization problem of Equation 1. The only weakness of CMH is their dependence to the extrinsic information; this limits our approach to shapes with the same (or very similar) poses. In [AK17] a geometry based regularization of the PCA basis has been proposed in order to improve the representation of the extrinsic coordinate functions. Nevertheless, similarly to our approach, these regularized PCA try to merge the intrinsic and the extrinsic representation of a mesh, they are based on the statistical analysis of a collection of data and can not be applied on a single mesh as done by our method.

Our proposed method is composed by the following 6 steps.

CMH: coordinates Manifold Harmonics (step1). Given a shape $\mathcal{M}$ and the set of its first $k_{\mathcal{M}}$ LBO eigenvectors $\boldsymbol{\Phi}_{k_{\mathcal{M}}} = [\boldsymbol{\phi}_1, \ldots, \boldsymbol{\phi}_{k_{\mathcal{M}}}]$. The coordinates Manifold Harmonics (CMH) are a set of $k_{\mathcal{M}} + 3$ orthonormal functions composed by the $k_{\mathcal{M}}$ first eigenfunctions of the LBO plus three new functions. We denote these three new functions with $\{\boldsymbol{\phi}_x, \boldsymbol{\phi}_y, \boldsymbol{\phi}_z\}$. We firstly introduce $\boldsymbol{\phi}_x$, then $\boldsymbol{\phi}_y$ and $\boldsymbol{\phi}_z$ are defined accordingly. Let $\boldsymbol{X}_{\mathcal{M}}$ be the x-coordinates of the vertices of $\mathcal{M}$. We compute $\widetilde{\boldsymbol{X}}_{\mathcal{M}}$ as the low-pass

Figure 3: *CMH construction. With respect to the 3D embedding we compute the difference in each coordinate between the original geometry and its low pass representation provided by the first MH (in our case 50 MH). On the right we visualize the three difference functions, each of which will generate a CMH function. Positive values are represented in red, negatives in blue and 0 in white.*

filter representation of $\boldsymbol{X}_{\mathcal{M}}$ provided by $\boldsymbol{\Phi}_{k_{\mathcal{M}}}$:

$$\widetilde{\boldsymbol{X}}_{\mathcal{M}} = \boldsymbol{\Phi}_{k_{\mathcal{M}}} \boldsymbol{\Phi}_{k_{\mathcal{M}}}^{\top} \boldsymbol{A}_{\mathcal{M}} \boldsymbol{X}_{\mathcal{M}}, \tag{2}$$

where $\boldsymbol{A}_{\mathcal{M}}$ is the mass matrix of $\mathcal{M}$. The representation error of $\boldsymbol{X}_{\mathcal{M}}$ is then defined as:

$$\boldsymbol{\Sigma} = \widetilde{\boldsymbol{X}}_{\mathcal{M}} - \boldsymbol{X}_{\mathcal{M}}. \tag{3}$$

The function $\boldsymbol{\phi}_x$ is defined as the orthogonal projection of $\boldsymbol{\Sigma}$ to the space spanned by $\boldsymbol{\Phi}_{k_{\mathcal{M}}}$:

$$\boldsymbol{\phi}_x = \boldsymbol{\Sigma} - \left(\boldsymbol{\Phi}_{k_{\mathcal{M}}} \boldsymbol{\Phi}_{k_{\mathcal{M}}}^{\top} \boldsymbol{A}_{\mathcal{M}} \boldsymbol{\Sigma} \right). \tag{4}$$

Finally we normalize $\boldsymbol{\phi}_x$:

$$\boldsymbol{\phi}_x = \frac{\boldsymbol{\phi}_x}{\|\boldsymbol{\phi}_x\|_{\mathcal{M}}}, \tag{5}$$

where $\|\boldsymbol{\phi}_x\|_{\mathcal{M}} = \sqrt{\langle \boldsymbol{\phi}_x, \boldsymbol{\phi}_x \rangle_{\mathcal{M}}} = \sqrt{\boldsymbol{\phi}_x^{\top} \boldsymbol{A}_{\mathcal{M}} \boldsymbol{\phi}_x}$. Now $\boldsymbol{\phi}_x$ is a function with norm equal to 1 that is orthogonal to $\boldsymbol{\Phi}_{k_{\mathcal{M}}}$. Adding $\boldsymbol{\phi}_x$ to $\boldsymbol{\Phi}_{k_{\mathcal{M}}}$ we update the set of orthonormal function as $\boldsymbol{\Phi}_{k_{\mathcal{M}}}^x = [\boldsymbol{\phi}_1, \ldots, \boldsymbol{\phi}_{k_{\mathcal{M}}}, \boldsymbol{\phi}_x]$. Then we can compute $\boldsymbol{\phi}_y$ substituting $\boldsymbol{X}_{\mathcal{M}}$ with $\boldsymbol{Y}_{\mathcal{M}}$ and $\boldsymbol{\Phi}_{k_{\mathcal{M}}}$ with $\boldsymbol{\Phi}_{k_{\mathcal{M}}}^x$ and applying all the steps in Equations 2, 3, 4 and 5. The same is done for $\boldsymbol{\phi}_z^{\mathcal{M}}$ substituting $\boldsymbol{Y}_{\mathcal{M}}$ with $\boldsymbol{Z}_{\mathcal{M}}$ and $\boldsymbol{\Phi}_{k_{\mathcal{M}}}^x$ with $\boldsymbol{\Phi}_{k_{\mathcal{M}}}^{x,y} = [\boldsymbol{\phi}_1, \ldots, \boldsymbol{\phi}_{k_{\mathcal{M}}}, \boldsymbol{\phi}_x, \boldsymbol{\phi}_y]$. The final set of orthonormal function, namely the *Coordinates Manifold Harmonics* (CMH) on $\mathcal{M}$ is given by $\boldsymbol{\Phi}_{k_{\mathcal{M}}}^{x,y,z} = [\boldsymbol{\phi}_1, \ldots, \boldsymbol{\phi}_{k_{\mathcal{M}}}, \boldsymbol{\phi}_x, \boldsymbol{\phi}_y, \boldsymbol{\phi}_z]$. It is worth noting that these new functions $\boldsymbol{\phi}_x, \boldsymbol{\phi}_y,$ and $\boldsymbol{\phi}_z$ encode, by definition, the essential extrinsic information to fully reconstruct the original shape (see Figure 2). In this fashion our CMH exploits the possibility to integrate intrinsic and extrinsic geometry of the surface $\mathcal{M}$ within the same spectral analysis framework. In Figure 4 we visualize an example of the CMH computed on two shapes.

Functional Map Estimation (step 2). Once the CMH basis are computed for $\mathcal{M}$ and $\mathcal{S}$ $\boldsymbol{\Phi}_{k_{\mathcal{M}}}^{x,y,z}$ and $\boldsymbol{\Psi}_{k_{\mathcal{S}}}^{x,y,z}$ respectively, we need to estimate a functional map $\boldsymbol{C}$ between $\mathcal{M}$ and $\mathcal{S}$ represented in these basis ($\boldsymbol{C} \in \mathbb{R}^{(k_{\mathcal{S}}+3) \times (k_{\mathcal{M}}+3)}$). Given two sets of probe functions $\mathbf{F} = [\boldsymbol{f}^{(1)}, \ldots, \boldsymbol{f}^{(q)}]$ on $\mathcal{M}$ and $\mathbf{G} = [\boldsymbol{g}^{(1)}, \ldots, \boldsymbol{g}^{(q)}]$ on $\mathcal{S}$, where $\boldsymbol{f}^{(p)}$ and $\boldsymbol{g}^{(p)}$ are correspondent functions defined respectively on $\mathcal{M}$ and $\mathcal{S}$, $\forall p \in \{1, \ldots, q\}$. We rely over the recent formulation proposed in [NO17], that requires to solve the following non-convex
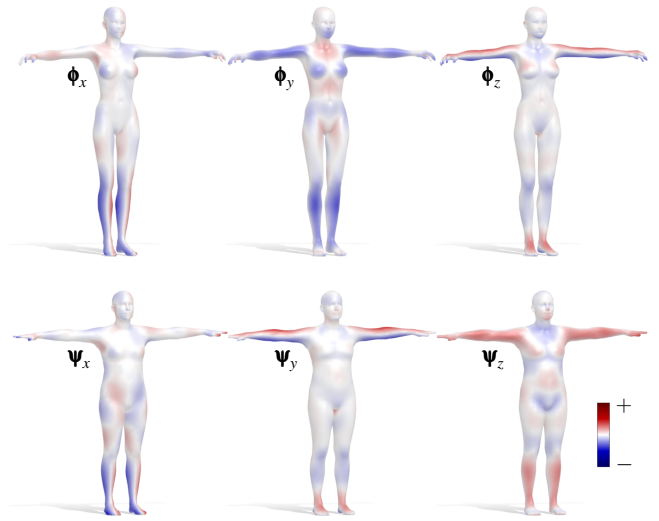
Figure 4: *CMH computed on two different shapes (a female shape from TOSCA [BBK08] and SMPL model [LMR*15]). As can be seen the order of the CMH is not shared by the two shapes. This is due to a different embedding in the 3D shapes, in other words the two shapes are not aligned and differ for a rigid transformation.*

optimization problem:

$$\min_{\boldsymbol{C}} \sum_p \|\boldsymbol{C}\hat{\mathbf{X}}^{(p)} - \hat{\mathbf{Y}}^{(p)}\boldsymbol{C}\|_F^2 + \gamma_1 \|\boldsymbol{C}\hat{\mathbf{F}} - \hat{\mathbf{G}}\|_F^2 + \gamma_2 \|\mathbf{C}\boldsymbol{\Lambda}_{\mathcal{M}} - \boldsymbol{\Lambda}_{\mathcal{S}}\boldsymbol{C}\|_F^2. \tag{6}$$

Equation 6 contains several characters:

- $\boldsymbol{\Lambda}_{\mathcal{M}}$ and $\boldsymbol{\Lambda}_{\mathcal{S}}$ are the diagonal matrices of the Laplacian eigenvalues associated with the basis functions.
- $\hat{\mathbf{F}}$ and $\hat{\mathbf{G}}$ are matrices containing the Fourier coefficients in the CMH basis of the given q probe functions placed side by side as columns of the matrices.
- $\hat{\mathbf{X}}^{(p)}$ and $\hat{\mathbf{Y}}^{(p)}$ are the commuting matrices, each associated to one of the two correspondent probe functions ($f^{(p)}, g^{(p)}$) represented in the reduced basis.
- γ_1 and γ_2 are empirical weights for energies.

	ϕ_x	ϕ_y	ϕ_z
ψ_x	0.8	0.1	0
ψ_y	0	0.1	1
ψ_z	0	−0.9	0.1
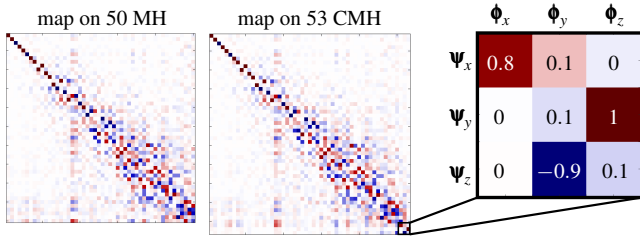
Figure 5: *A comparison between functional maps. From left to right: the maps computed for the first 50 eigenfunctions, the map computed for the proposed CMH, a detail of the coefficients that represent how the 3 new basis are mapped from one shape to the other. This maps are estimated for the pair visualized in Figure 4. As can be seen the map computed on the CMH solves for the switches of the CMH functions. Red encodes values close to 1, blue close to −1 while white is equal to 0.*

For all our experiments we set $\gamma_1 = 0.1$ and $\gamma_2 = 0.001$.

The selection of probe functions is fundamental since it leads the energy and the optimization. In particular the selected functions should describe well global and local geometry of the surfaces. It is desirable that they are stable with respect to the deformations (both isometric and non-isometric). The problem still open and several solutions has been proposed. Descriptors (e.g. HKS [SOG09] [GBAL09] and WKS [ASC11]) are widely adopted in this context. Another standard choice involves the use of landmarks, usually diffused by some propagation techniques (e.g. heat diffusion). Usually these landmarks require supervised selection, but for human body they can be automatically selected through the method proposed in [MMRC18] based on the discrete time evolution process theory introduced in [MOR*18]. We use these landmarks and WKS descriptors for all our experiments. An example is depicted in Figure 5, that shows the map estimated using the CMH compared to the standard functional map.

Point mapping and first mesh generation (step 3). Given the functional map $\boldsymbol{C}$, as stated in [OBCS*12] we convert it in a point-to-point map $\boldsymbol{\Pi} : \mathcal{S} \to \mathcal{M}$ solving $\forall s \in \mathcal{S}$ the following nearest neighbor assignment in the spectral domain:

$$\boldsymbol{\Pi}(s) = \arg\min_{m \in \mathcal{M}} \|\boldsymbol{C}\boldsymbol{\Phi}_{k_\mathcal{M}}^{x,y,z}(m) - \boldsymbol{\Psi}_{k_\mathcal{S}}^{x,y,z}(s)\|_F \quad (7)$$

Hands refinement through local correspondence (step 4). Once we have the correspondence $\boldsymbol{\Pi}$, we would refine this correspondence in local regions that correspond to the hands, denoted as $H(\mathcal{S})$, where usually the error is large. As done in [MMRC18], we define a local geodesic ball around hands and then we register them using Coherent Point Drift (CPD) approach proposed in [MS10] which returns a local correspondence on the hands $\boldsymbol{\Pi}_{cpd}$. Merging global and local correspondences we obtain $\boldsymbol{\Pi}_{final}$, the correspondence defined as:

$$\boldsymbol{\Pi}_{final}(x) = \begin{cases} \Pi_{cpd}(x) & x \in H(\mathcal{S}) \\ \Pi(x) & \text{otherwise} \end{cases} \quad (8)$$

We use this correspondence to transfer the mesh. Note there is no

guarantees that meshes have the same number of vertices. Furthermore, a vertex-to-vertex correspondence is a really constrained solution, and can lead to undesired collapsing, flipping and others artifacts.

For this reason we would provide to our pipeline the possibility to generate solutions different from the vertex-to-vertex ones. From now on we adopt the following notation

- $\mathcal{S}$: the shape with the desired connectivity.
- $\mathcal{M}$: the shape that represent the geometry we want to fit.
- $\mathcal{M}_\mathcal{S}$: the shape with the geometry of $\mathcal{M}$ and the connectivity of $\mathcal{S}$.

ARAP for connectivity consistency (step 5). In this step we switch from the functional domain to the euclidean one. We regularize the transferred connectivity in an as-rigid-as-possible formulation as proposed in [CPSS10]. Considering the following energy:

$$E_{arap} = \frac{1}{4} \sum_{e_{ij} \in \mathcal{E}} \cot \alpha_{ij} |q_{ij} - R p_{ij}|^2 \quad (9)$$

where $p_{ij} = i - j$, q_{ij} is the value of p_{ij} in the new configuration and R_{ij} is the rotation that best approximates the transformation occurred between the two configurations. In [CPSS10] the authors provide a gradient derivation for the energy 9. This energy measures how far we are from a rigid transformation and encourage the vertices neighborhoods to find an elastic equilibrium. In our case, we decide to apply this energy between the mesh $\mathcal{S}$ and the new vertices positions obtained from $\mathcal{M}_\mathcal{S}$.

This approach has two main advantages: firstly, as-rigid-as possible approach fosters local rigidity and help to solve inconsistent situations derived from vertices transfer. Secondly, it can be efficiently optimized by gradient techniques. The optimization tends to fall in a local minimum without ruins the global correspondence achieved before.

Finally, note that for now we are not requiring to fit the geometry of $\mathcal{M}$. In some cases it is reasonable, because changing the connectivity of a model means also a different discretization of the underlying geometry. On the other hand, some local undesired deformation from original geometry could appear.

ARAP for geometry fitting (step 6). The geometry that we obtain should be close to the one we desire, but some artifacts can still arise: they may be caused by pose misalignment between two models (e.g. difference in the neutral pose between two subjects), noise in correspondence and also by stitching the $\boldsymbol{\Pi}$ with $\boldsymbol{\Pi}_{cpd}$. All these issues are transformed in a coherent continuous surface by previous ARAP step and we do not expect huge artifacts (e.g. intersections, triangles flipping). In the worst cases, the surface has been collapsed in some points and need to be inflated, or the ARAP regularization of connectivity has sensibly modified local details of geometry.

For these reasons, we perform a final local registration:

$$E_{reg} = w_a E_{arap} + w_d E_{dato} \quad (10)$$

where E_{arap} is defined as in Equation 9 (we still require the coherence with the original mesh). E_{dato} is defined as:

$$E_{dato} = \sum_{i \in \mathcal{V}_{\mathcal{M}_\mathcal{S}}} \min_{x \in \mathcal{M}} ||i - x||^2 \quad (11)$$

Geometry   Connectivity   Geometry + Connectivity
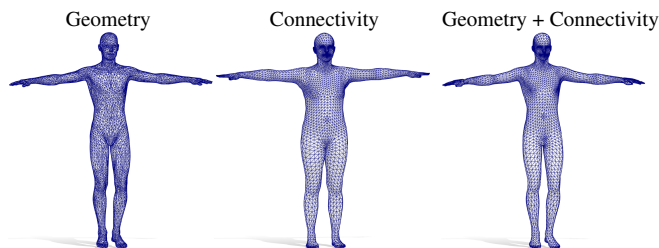
Figure 6: *Qualitative results on the transfer of SMPL model connectivity to david0 geometry from TOSCA dataset.*

Geometry   Connectivity   Geometry + Connectivity

Figure 7: *Connectivity transfer example for a non-standard pose from SMPL model to a shape from SMPL 3K dataset.*

where x is a point on the surface of $\mathcal{M}$. This energy can be read as a vertex-to-surface distance and is important to approximate the geometry of $\mathcal{M}$. The weights w_a and w_d are chosen empirically; in our experiments we found that 0.3 and 1 respectively provide a stable setup. We optimize E_{reg} using a gradient technique. The optimal solution leads to the final $\mathcal{M}_\mathcal{S}$; a model that shares the connectivity of $\mathcal{S}$ and approximates the geometry of $\mathcal{M}$.

5. Results

In this Section we evaluate our method through several experiments and applications.

Data. Here we briefly list the data involved in our experiments. **SMPL model** [LMR*15] is a widely used parametric model of human body represented as triangular mesh with 6890 vertices. With this model we are able to generate several different human shapes that share a common pose and connectivity; we will refer to these shapes as **SMPL dataset**. **FAUST** [BRLB14] is a dataset that shares the same connectivity of SMPL. It is composed of 100 shapes from 10 different subjects in the same 10 different poses. For all these shape the ground truth correspondence is provided. **TOSCA** [BBK08] a synthetic dataset that contains different classes including 3 human shapes (2 male and 1 female). All the shapes in the same class share the same connectivity. **MakeHumans** [BRM08] is an open source software for human body generation. Varying the parameters it is possible to obtain different shapes and details of the human shapes. We refer to shapes generated by this tool as **MakeHumans**.

Connectivity transfer. We perform several qualitative and quantitative connectivity transfer experiments involving pairs with heterogeneous characteristics. Some qualitative results can be seen in Figures 1, 6, 7, and 9

The qualitative example in Figure 7, for the transfer of the SMPL model connectivity to a shape from the SMPL 3K dataset, shows that Our method provides a high quality connectivity transfer also for a low resolution mesh with a non-standard pose.

Comparison with other methods. The proposed pipeline provides a valuable improvement, and we show a quantitative comparison with other possible baselines. As competitors we consider:

MH: it corresponds to our pipeline applied on a standard functional map of size 53×53 defined on the manifold harmonics.
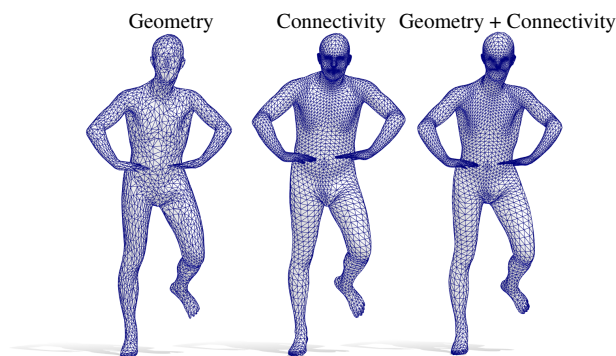
This is a reasonable competitor because is immediate, fast and relies on our same assumptions.

LMH: as above, it is our pipeline applied on a functional map of size 53×53 defined on the 50 standard manifold harmonics, plus 3 localized manifold harmonics defined as in [MRCB18]. This is more sophisticated than the previous bullet, and addresses directly the representation of the shape in a local sense.

D&D: We apply the refinement proposed in [EBC17] to a functional map of size 53×53. The refinement produces a correspondence that can lie inside the faces, and then these points are used as vertices of the new mesh. Nowadays this represents the state of the art in the vertex-to-point mapping relying on functional map theory. We found interesting to compare it to our method, because our use of ARAP produces similar freedom in the vertices placement.

All the functional maps used in these experiments are estimated through the method proposed in [NO17] using the same probe functions and landmarks. The results depicted in Figure 8 show that the proposed CMH are better suited for this task with respect to both MH and LMH. Furthermore our pipeline applied on all the three bases provides results that outperform the state of the art refinement methods.

Attributes transfer in graphic pipeline. In modelling and animation frameworks it is often required to effectively transfer model attributes such as textures or skinning properties among different shapes. To this aim, one of the most used morphable model is SMPL, a data-driven model, equipped with a great amount of ready-to-use properties such as animation information. However, it is not provided of a texture, and also its resolution is limited by its vertices (i.e., 6890). On the other side replicate the learning phase is expensive and complicated. To overcome these limits, we applied our pipeline to the standard T-posed SMPL template, to substitute it with a more graphical appealing one, obtained by Autodesk Character's Generator. This let us to transfer a texture and to increase the number of vertices improving the resolution. In the same time by keeping the original SMPL geometry we can transfer the ready-to-use properties learned for SMPL and apply them to the new connectivity. We apply nearest-neighbor between the two aligned sur-
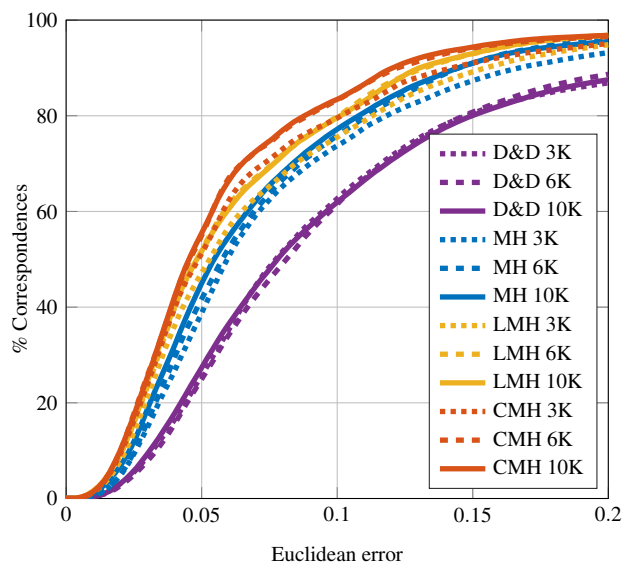
Figure 8: *Comparison on the SMPL dataset. The results are on average on 10 shapes remesh with the SMPL connectivity. Solid lines represent results on 10K vertices shapes, dashed lines results on meshes with 6K vertices and dotted ones on meshes with 3K vertices.*

faces to transfer the animation information. The obtained results are exciting, and we are able to generate more zombie-like models as illustrated in Figure 10.

6. Conclusions

In this paper we propose a new approach for surface remeshing based on a fully automatic shape matching strategy. We have shown that with our method is possible to obtain a very regular mesh that satisfies the constraints for a professional use starting from the geometry observed on a given human-shape and inheriting the correct tessellation from another subject with similar pose. Our main contribution is the definition of a new set of basis functions, namely the *coordinates manifold harmonics* (CMH) that are properly designed to improve the functional correspondence and to exploit the effectiveness of merging intrinsic and extrinsic information within the same spectral matching framework. Our exhaustive experimental section has reported the improvement of our method in transfering the desired connectivity on previously unseen geometry for different applicative domains in comparison with other approaches.

The main limitation of our method is that we need to match the input shape with a target subject with the same pose. Although in this paper we focused only on human body shapes our method, and in particular our CMH formulation, can be easily extended to work on different classes of shape. Furthermore, the proposed pipeline can be also exploited for the point-to-point matching application, directly computing the Euclidean nearest neighbour of each point between the original vertices that represent the geometry and the vertices of the transferred connectivity. In this paper we focus on the mesh transfer application but we leave the point-to-point match-

ing application as future direction. Finally thanks to the flexibility of the functional maps framework as future work we aim to adopt the CMH tool in the case of topological error or for partial shapes through the partial functional maps framework [RCB*17].

References

[ABCCO13] AZENCOT O., BEN-CHEN M., CHAZAL F., OVSJANIKOV M.: An operator approach to tangent vector field processing. In *Computer Graphics Forum* (2013), vol. 32, pp. 73–82. 2

[ACBCO17] AZENCOT O., CORMAN E., BEN-CHEN M., OVSJANIKOV M.: Consistent functional cross field design for mesh quadrangulation. *ACM Trans. Graph. 36*, 4 (July 2017), 92:1–92:13. 2

[AK17] AFLALO Y., KIMMEL R.: Regularized principal component analysis. *Chinese Annals of Mathematics, Series B 38*, 1 (Jan 2017), 1–12. 2, 3

[ASC11] AUBRY M., SCHLICKEWEI U., CREMERS D.: The wave kernel signature: A quantum mechanical approach to shape analysis. In *Proc. ICCV* (Barcelona, Spain, 2011), IEEE, pp. 1626–1633. 5

[BBK08] BRONSTEIN A. M., BRONSTEIN M. M., KIMMEL R.: *Numerical Geometry of Non-Rigid Shapes*. Springer, 2008. 4, 6

[BMR*99] BERNARDINI F., MITTLEMAN J., RUSHMEIER H., SILVA C., TAUBIN G.: The ball-pivoting algorithm for surface reconstruction. *IEEE Transactions on Visualization and Computer Graphics 5*, 4 (Oct 1999), 349–359. 2

[BRLB14] BOGO F., ROMERO J., LOPER M., BLACK M. J.: FAUST: Dataset and Evaluation for 3d Mesh Registration. In *Proc. CVPR* (2014), pp. 3794–3801. 6

[BRM08] BASTIONI M., RE S., MISRA S.: Ideas and methods for modeling 3d human figures: The principal algorithms used by makehuman and their implementation in a new approach to parametric modeling. In *Proceedings of the 1st Bangalore Annual Compute Conference* (New York, NY, USA, 2008), COMPUTE '08, ACM, pp. 10:1–10:6. 6

[BZK09] BOMMES D., ZIMMER H., KOBBELT L.: Mixed-integer quadrangulation. *ACM Trans. Graph. 28*, 3 (July 2009), 77:1–77:10. 2

[CPSS10] CHAO I., PINKALL U., SANAN P., SCHRÖDER P.: A simple geometric model for elastic deformations. In *ACM transactions on graphics (TOG)* (2010), vol. 29, ACM, p. 38. 5

[CSBK16] CHOUKROUN Y., SHTERN A., BRONSTEIN A., KIMMEL R.: Hamiltonian operator for spectral shape analysis. *arXiv:1611.01990* (2016). 2

[EBC17] EZUZ D., BEN-CHEN M.: Deblurring and denoising of maps between shapes. *Computer Graphics Forum 36*, 5 (2017), 165–174. 2, 6

[GBAL09] GEBAL K., BÆRENTZEN J. A., ANÆS H., LARSEN R.: Shape analysis using the auto diffusion function. *Computer Graphics Forum 28*, 5 (2009), 1405–1413. 5

[JTPSH15] JAKOB W., TARINI M., PANOZZO D., SORKINE-HORNUNG O.: Instant field-aligned meshes. *ACM Transactions on Graphics (Proceedings of SIGGRAPH ASIA) 34*, 6 (Nov. 2015). 2

[LMR*15] LOPER M., MAHMOOD N., ROMERO J., PONS-MOLL G., BLACK M. J.: SMPL: A skinned multi-person linear model. *ACM Trans. Graph. 34*, 6 (2015), 248:1–248:16. 4, 6

[MMRC18] MARIN R., MELZI S., RODOLÀ E., CASTELLANI U.: Farm: Functional automatic registration method for 3d human bodies. *arXiv preprint arXiv:1807.10517* (2018). 5

[MOR*18] MELZI S., OVSJANIKOV M., ROFFO G., CRISTANI M., CASTELLANI U.: Discrete time evolution process descriptor for shape analysis and matching. *ACM Transactions on Graphics (TOG) 37*, 1 (Jan. 2018), 4:1–4:18. 5

[MPP*13] MARCIAS G., PIETRONI N., PANOZZO D., PUPPO E., SORKINE-HORNUNG O.: Animation-aware quadrangulation. In *Proceedings of the Eleventh Eurographics/ACMSIGGRAPH Symposium on*

Connectivity   Texture   Geometry   Connectivity + Texture + Geometry
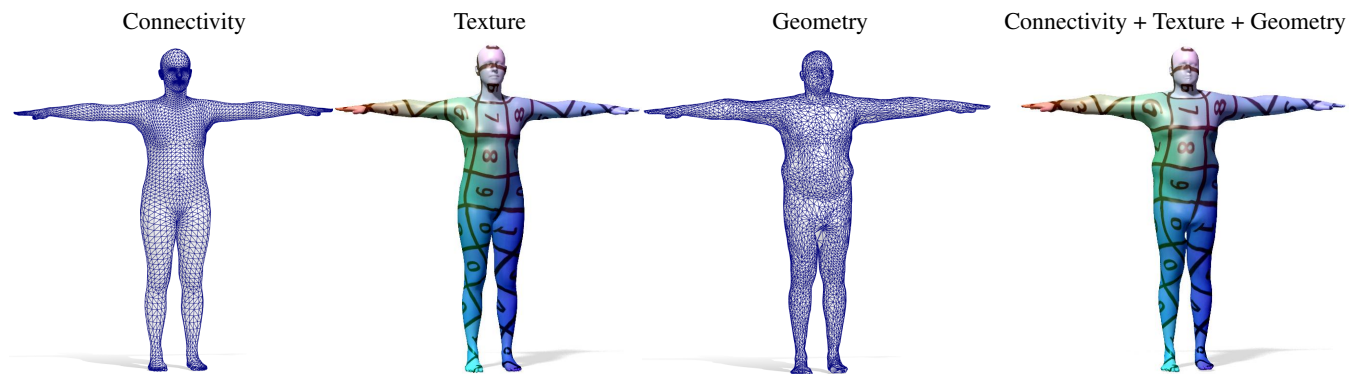
Figure 9: *An example of texture transfer between models. From the left: a regular connectivity, a defined texture and an irregular geometry we desire to texturize. On the right the result. We would like to underlie that transferring good connectivity let the geometry to inherit some desirable properties (e.g. face and feet details).*

Geometry   Connectivity+Texture   Geometry+Connectivity+Texture   Animated Results
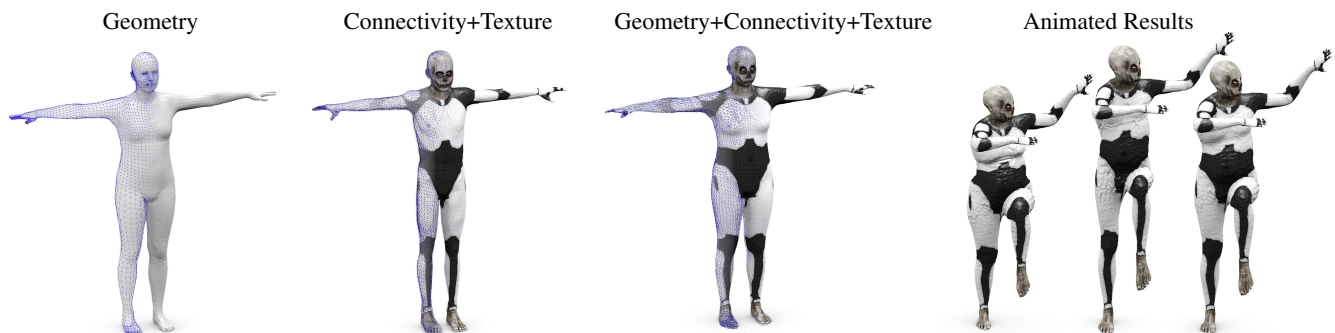
Figure 10: *The model substitution experiment. From left to right: the SMPL model that provide the geometry, an Autodesk's Character Generator model (around 10K vertices) that provides the connectivity and the texture; the result of our transfer and some model generated by including our output inside SMPL framework. We are able to* automatic *substitute the SMPL template with an arbitrary one, generating many texturized and shaped models, and move them using inherited skinning information.*

Geometry Processing (Aire-la-Ville, Switzerland, Switzerland, 2013), SGP '13, Eurographics Association, pp. 167–175. 2

[MRCB18] MELZI S., RODOLÀ E., CASTELLANI U., BRONSTEIN M. M.: Localized manifold harmonics for spectral shape analysis. *Computer Graphics Forum 37*, 6 (2018), 20–34. 2, 6

[MS10] MYRONENKO A., SONG X.: Point set registration: Coherent point drift. *IEEE transactions on pattern analysis and machine intelligence 32*, 12 (2010), 2262–2275. 5

[MTP*15] MARCIAS G., TAKAYAMA K., PIETRONI N., PANOZZO D., SORKINE-HORNUNG O., PUPPO E., CIGNONI P.: Data-driven interactive quadrangulation. *ACM Trans. Graph. 34*, 4 (July 2015), 65:1–65:10. 2

[NMR*18] NOGNENG D., MELZI S., RODOLÀ E., CASTELLANI U., BRONSTEIN M., OVSJANIKOV M.: Improved functional mappings via product preservation. *Computer Graphics Forum 37*, 2 (2018), 179–190. 2

[NO17] NOGNENG D., OVSJANIKOV M.: Informative Descriptor Preservation via Commutativity for Shape Matching. *Computer Graphics Forum* (2017). 2, 4, 6

[OBCS*12] OVSJANIKOV M., BEN-CHEN M., SOLOMON J., BUTSCHER A., GUIBAS L.: Functional maps: a flexible repre-

sentation of maps between shapes. *ACM Transactions on Graphics (TOG) 31*, 4 (2012), 30:1–30:11. 2, 3, 5

[OCB*16] OVSJANIKOV M., CORMAN E., BRONSTEIN M., RODOLÀ E., BEN-CHEN M., GUIBAS L., CHAZAL F., BRONSTEIN A.: Computing and processing correspondences with functional maps. In *SIGGRAPH ASIA 2016 Courses* (2016), pp. 9:1–9:60. 3

[PP93] PINKALL U., POLTHIER K.: Computing Discrete Minimal Surfaces and their Conjugates. *Experimental mathematics 2*, 1 (1993), 15–36. 3

[PTC10] PIETRONI N., TARINI M., CIGNONI P.: Almost isometric mesh parameterization through abstract domains. *IEEE Transaction on Visualization and Computer Graphics 16*, 4 (July/August 2010), 621–635. 2

[RCB*17] RODOLÀ E., COSMO L., BRONSTEIN M. M., TORSELLO A., CREMERS D.: Partial functional correspondence. *Computer Graphics Forum 36*, 1 (2017), 222–236. 7

[SOG09] SUN J., OVSJANIKOV M., GUIBAS L. J.: A concise and provably informative multi-scale signature based on heat diffusion. *Computer Graphics Forum 28*, 5 (2009), 1383–1392. 5